Microscopic and mineralogical characteristics behind the engineering properties of a compacted andesitic volcanic soil

Highlights

- Drying procedure influences engineering behaviour of volcanic soils
- Key to the understanding of volcanic soil's behaviour lies in its mineralogy
- Halloysite dehydration at mineral scale explains drying's impact on behaviour

Abstract

Most of the volcanic soils found around the world are concentrated in regions of high demographic and economic growth. Research shows that the drying process to which volcanic soil samples are subjected to as part of the preparation process for laboratory testing can affect soil engineering behaviour, inadvertently leading to undesirable results. Previous studies suggest that the key to the understanding of the behaviour of volcanic soils lies in its mineralogy. Thus, this paper proposes an experimental investigation on an andesitic volcanic soil from Popayan, Colombia, to investigate the extent to which changes in drying affect the engineering behaviour of the soil. Mineralogical tests indicated the presence of halloysite in the soil. From the geotechnical, hydromechanical and structural tests it was possible to recognise that the drying procedure influenced: compaction behaviour; consistency limits; particle size distribution; retention behaviour; compressibility and pore size distribution (> 1 μm), while not having great effect on: specific surface; pore size distribution (< 1 μm). Combined analyses of the laboratory tests performed suggested that the dehydration of halloysite at mineral scale could then explain the distinct change in engineering behaviour observed when this soil is subjected to drying.

Key words: volcanic soil, halloysite, hydromechanical, mineralogy, particle size distribution, pore size distribution.

1. Introduction

Volcanic soils cover 1% of the Earth's surface yet they support 10% of the world's population, including some of the highest human population densities (Neall, 2009; Soil Survey Staff, 1998). Andesitic

This is a peer-reviewed, accepted author manuscript of the following article: Hernandez Menendez, O., De Carvalho Faria Lima Lopes, B., Caicedo, B., & Porfirio Cordão-Neto , M. (2022). Microscopic and mineralogical characteristics behind the engineering properties of a compacted andesitic volcanic soil. Journal of South American Earth Sciences, 115, [103752]. https://doi.org/10.1016/j.jsames.2022.103752

volcanism is at the origin of volcanic soils that rim the Pacific. They cover ample areas of Chile, Peru, Ecuador, Colombia, Central America, the United States, Kamchatka, Japan, the Philippines, Indonesia, New Zealand, and the independent island states of the southwest Pacific. Approximately 60% of them are in regions of tropical climate (Shoji et al., 1993).

Early volcanic soils are composed mainly of volcanic glass; in such soils, the very rapid cooling inhibits the development of a crystalline structure in the fine molten particles. This rapid cooling forms distinctive clays, such as allophanes, having a "weak" degree of crystallinity (referred to as "short-range order clays" or SROC). Afterward, on weathering, the amount of SROCs decreases, and the amount of clays like halloysite and gibbsite increase. Then, more advanced stages of weathering transform halloysites into kaolinite (Wesley, 2014).

Andisols are a special category of volcanic soils that have particular engineering properties, mainly when they undergo weathering under tropical conditions (Neall, 2009). The main challenges regarding these soils are related to the stability of natural slopes (Betancur et al., 2013; Terlien, 1997), erosions (Bommer et al., 2002) and difficulties in the compaction process (Almazán, 2013; Hernandez et al., 2018; Wesley, 2009). Several studies demonstrated that the geotechnical properties of volcanic soils are different from region to region of origin (Betancur et al., 2013; Terlien, 1997).

Regarding their engineering properties, Andisols are characterized by a high macro-porosity, high natural water content, and very low bulk density (≤ 0.90 Mg m^{-3}). Moreover, these soils suffer marked texture changes from a smeary gel at field water content to an apparent sandy soil with no cohesion when air dried. Additionally, air drying also affects: soil classification (particle size distribution); Atterberg limits and compaction properties (Wesley, 2014; 2009; 1973 and Hernandez et al., 2018). This in turn can lead to changes in hydromechanical (Colombo et al. 2014; De Vita et al. 2012; Dorel et al. 2000; Emmanuel et al. 2019; Joussein et al. 2006), structural (Bartoli et al. 2007; Emmanuel et al. 2019; Hernandez et al. 2018) and cyclic (Matsumura et al. 2015) responses. Hernandez et al. (2018), Colombo et al. (2014) and De Vita et al. (2012) suggested that the key to the understanding of the behaviour of the volcanic soil lies in its mineralogy.

Kitagawa (1971) and Dörner et al. (2009) have attributed the irreversible drying and hysteresis between dehydration and rehydration of volcanic ash soils observed by other researchers to the allophane. Poulenard et al. (2003) observed that Andisols will become especially fragile if handled and that the irreversible loss of their water holding capacity will likely induce phenomena that are harmful to soil quality, according to them the largest part of the water holding capacity of these materials is therefore associated with the water stored in those fine and very fine pores. Similarly, Wesley (1973)

reached the conclusion that the nature of the individual particles (of the halloysite) and the 'gel' (of the allophane) were the main factors that contributed to the unusual engineering properties of the volcanic soils investigated by the author. However, the extent to which the mineralogy plays a role on the behaviour of volcanic soils still needs further investigation.

Thus, this paper explores this link between the mineralogy and the geotechnical change in behaviour and response of an andesitic volcanic soil when samples are subjected to different drying preparation procedures. Results of an experimental investigation carried out on a volcanic soil from Popayan, Colombia, are presented. Firstly, mineralogical tests, were performed to assess the mineralogical composition of soil samples subjected to different drying procedures when appropriate. Then, to investigate the extent to which changes in drying affect the engineering behaviour of the soil, geotechnical, hydromechanical and structural characterization tests were carried out on compacted (following different drying preparation procedures) and intact soil samples. Only the combined analyses of these findings would allow an insight into aspects that have already been discussed in other publications, such as the significant variation in field and laboratory behaviour.

2. Material and methods

2.1. Material

The material used for this study was a volcanic ash from Popayán, Colombia, located 80km from Puracé volcano, where the climate is classified as temperate and humid (Hurtado, 2014). Colombia's volcanic ash soils from a few meters depth are typically yellowish coffee in colour, composed of highly plasticity clays, originated from volcanic ash sediments deposited over 4,000 years ago (Lizcano et al., 2006). For this study, samples were collected (disturbed and intact block) from a depth of 2m in November, which is historically the month with the highest average precipitations.

2.2. Experimental procedure and specimen preparation

The experimental procedure and specimen preparation adopted are illustrated in **Fig. 1**. Three different specimens were prepared: the intact specimen, moulded from the intact block. Procedure A involved air drying the disturbed soil up to the target water content required, breaking soil lumps with the help of a pestle and mortar, sieving the material in sieve #10 (2mm) and sealing it into a plastic bag for 24hrs for homogenisation. Procedure B involved air drying the disturbed soil to the hygroscopic water content, breaking soil lumps with the help of a pestle and mortar, sieving the material in sieve #10 (2mm), moistening the material to the target water content when appropriate and finally sealing

139 it into a plastic bag for 24hrs for homogenisation. Procedure A is the procedure usually followed in the
140 field, while procedure B is conventionally required by international standard for laboratory testing.

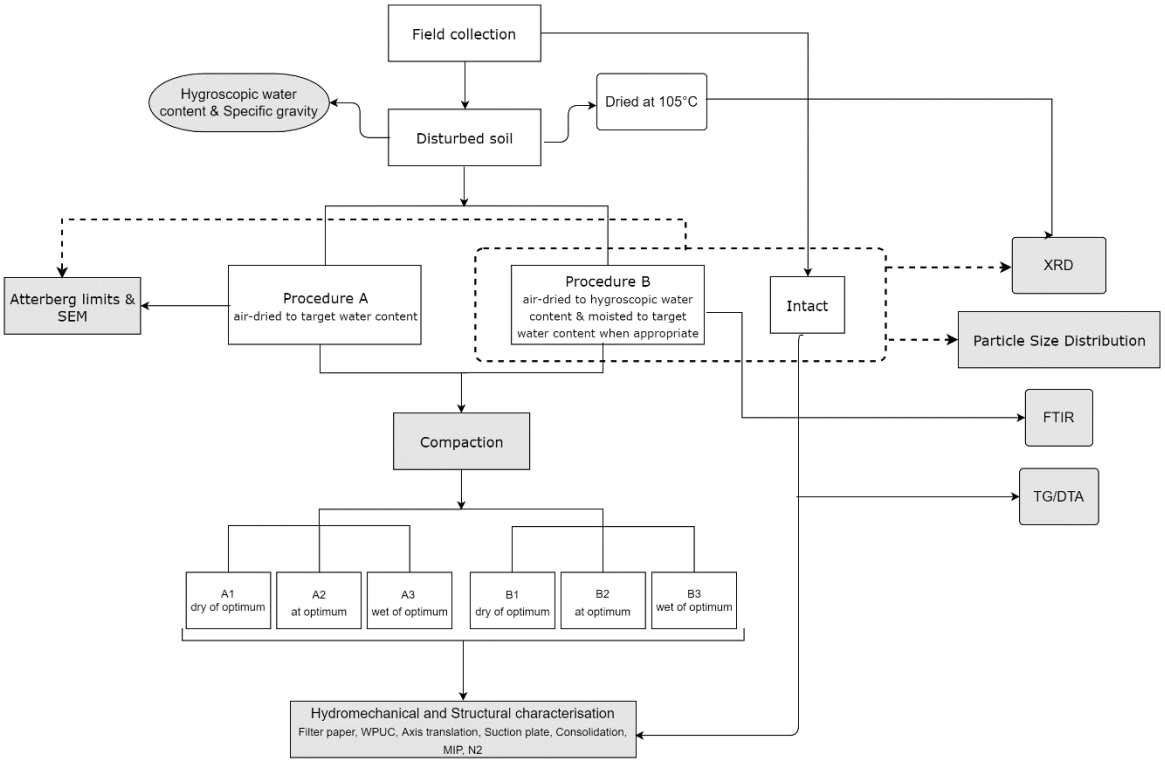

141

142 ***Fig. 1****. Experimental procedure and specimen preparation.*

143 The hygroscopic water content was determined according to the procedure suggested by Shah and
144 Singh (2005) and the value obtained was 7.70% at the relative humidity and temperature of the
145 laboratory, approximately 37% at 24 °C respectively. The specific gravity was determined following
146 ASTM D854-14 (2014) and the value obtained was 2.59.

147 As noted by Wesley (2009) and Hernandez et al. (2018) soils of volcanic origin are sensitive to the
148 drying process presenting a large and rapid variation in optimum water content. To analyse this
149 variability, samples were compacted with energy corresponding to the Standard Proctor (NBR 7182,
150 2016; ASTM D698, 2012), using specimen preparation methods A and B, as previously described (**Fig.**
151 **1**). From these procedures, two compaction curves were obtained, as shown in **Fig. 2**.

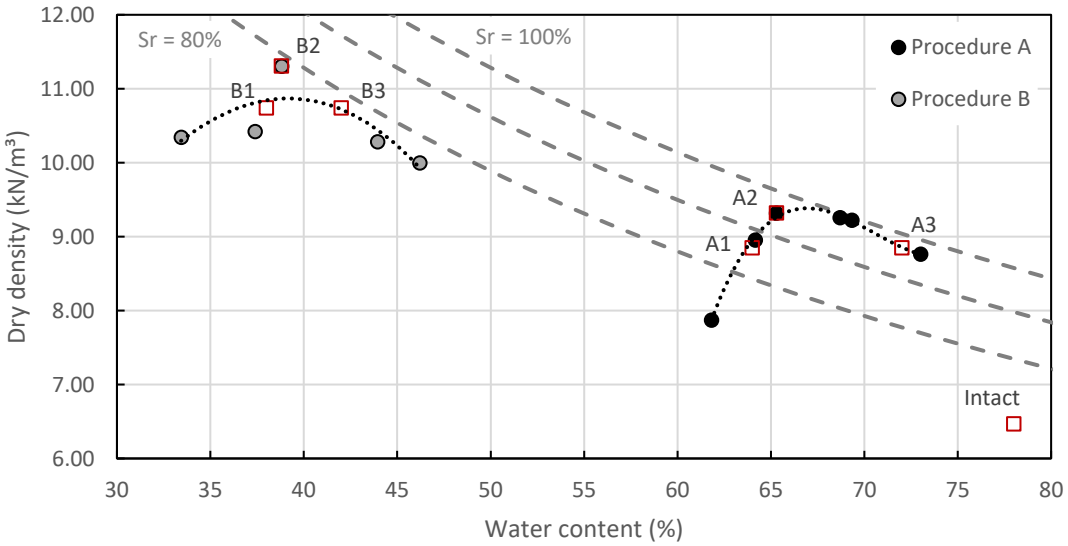

Fig. 2. *Standard Proctor compaction curves of procedure A and B.*

The points of interest were defined from the two compaction curves. Three points were used for each compaction curve: on the dry of optimum (95% of the optimum dry density, A1 and B1), at optimum (A2 and B2), and on the wet of optimum (95 % of the optimum dry density, A3 and B3). **Table 1** shows the characteristics of each specimen. The porosity, degree of saturation and void ratio of the samples air dried to the hygroscopic water content (Procedure B) are lower than the samples prepared according to procedure A (without substantial drying), which demonstrates the influence of drying on the change in soil structure. **Fig. 2** also shows the dry density and water content of the intact specimen (6.47 kN/m³ and 78.0%).

Table 1 *Sample characteristics.*

Sample	Water content, w (%)	Dry unit weight, γ_d (kN/m^3)	Initial void ratio, e_i	Degree of saturation, Sr (%)	Porosity, n	Suction, s (kPa)
Intact	78.0	6.47	2.95	68.5	0.74	298
A1	64.0	8.85	1.93	85.9	0.66	150
A2	65.3	9.32	1.78	95.1	0.64	210
A3	72.0	8.85	1.91	97.1	0.66	170
B1	38.0	10.74	1.42	69.3	0.59	29
B2	38.8	11.31	1.30	77.8	0.56	11
B3	42.0	10.74	1.42	76.6	0.59	17

2.2.1. Mineralogical characterisation

As a first qualitative assessment of the morphology of the material tested, Scanning Electron Microscopy (SEM) images were carried out. Specimens of the intact and compacted samples were air

dried to the hydroscopic water content, soil lumps were broken while the material was sieved (0.075mm) manually and they were coated with gold. SEM images were performed with JJSM 700 1F equipment.

For the mineralogical characterisation, X-Ray Diffraction (XRD), Thermogravimetric Analyses (TG/DTA) and Fourier Transform Infrared Spectroscopy (FTIR) tests were carried out.

Three specimens were prepared for XRD tests. The first one was prepared by oven drying the disturbed soil at 105 °C, the second specimen was air-dried to the hygroscopic water content and the last specimen was obtained from the intact block and kept moist at water content equal to 78%. Then these 2 dried specimens were crushed and sieved (0.075mm), while the moist specimen was only crushed to maintain the conditions found in the field. XRD analyses were carried out in the RIGAKU - ULTIMA IV diffractometer, using copper tube and nickel filter. In the test, a wave with a length of 1.54 Å and a scanning speed of 0.05 °/min were used. From the diffractograms, minerals were identified, with support from the MDI JADE 9.0 software.

Thermogravimetric analyses (TG/DTA) were used to study the kinetics of any phase transformation processes and chemical reaction mechanisms up to 900°C with a heating rate of 10 °C/min. The equipment used was the DTG-60H. TG/DTA is a technique that measures the variation in mass when a material is subjected to the heating process in a controlled (inert) atmosphere. Therefore, this technique does not allow identifying the mineralogical change due to the drying preparation process. Hence, only specimens obtained from the intact block underwent TG/DTA testing.

Complementarily to the XRD and TG/DTA analyses, FTIR tests were performed using the VERTEX 70 equipment. A specimen obtained from the disturbed sample was air dried to the hydroscopic water content crushed and sieved (0.075mm). Then, 1g of soil was mixed with 5g of Potassium bromide (KBr) to prepare the tablets that were subjected to analyses. Finally, a software was used to identify the absorbance spectra for each wave number, which then identifies the different existing minerals by the length of the wave.

2.2.2. Geotechnical characterisation

Geotechnical characterisation tests included: particle size distribution, with and without dispersant and Atterberg limits. Sieving and sedimentation were employed to the determination of the particle size distribution. These tests were carried out on intact specimens and specimens prepared according to procedure B (air-dried to hygroscopic water content) following ASTM D6913/D6913M-17 (2017) for sieving and ASTM D7928 (2017) for sedimentation, with and without dispersant. The Atterberg limits were determined following ASTM D4318-17 (2017) for the intact specimen and specimens that

underwent preparation procedure A (air-dried to 65.3% and then wetted) and procedure B (air-dried to hygroscopic water content and then wetted).

2.2.3. Hydromechanical characterisation

The hydraulic behaviour was assessed via the Soil Water Retention Curve (SWRC). The SWRC was measured for the entire suction range following drying and wetting paths. To determine the SWRC on the drying path, three techniques were used: suction plate (1-15kPa), axis translation (20-200kPa) and dewpoint psychrometer, WP4C (40kPa-300MPa). Before each test, specimens moulded from intact and compacted (A1 to A3, B1 to B3) samples were saturated. The dimensions of specimens were: 2.5x1.0 cm, 6.5x2.0 cm and 5.0x0.5 cm (diameter x height) for suction plate, axis translation and WP4C, respectively. For the wetting path, only WP4C technique was used.

Compressibility was evaluated through consolidation tests, carried out according to ASTM D2435/D2435M (2020). Specimens of 5.0 cm in diameter and 2.0 cm in height moulded from intact and compacted (A1 to A3, B1 to B3) samples were first saturated and then subjected to successive increments of vertical stress, starting from 10kPa. Stresses were doubled at each new step up to 1,200kPa. Unloading steps, back to 10kPa, took place in similar fashion.

2.2.4. Structural characterisation

To assess the structural behaviour, porosimetry tests were carried out by adsorption and desorption of nitrogen and Mercury Intrusion Porosimetry (MIP).

For porosimetry by adsorption and desorption of nitrogen, cubic specimens of approximately 7mm were moulded from intact and compacted (A1 to A3, B1 to B3) samples, placed in the oven for 7 days at a temperature of 105 °C, followed by freezing in liquid nitrogen (-195 °C) and drying in a vacuum oven. The Nova 2200e porosimeter from Quantachrome instrument was used for this test.

For the MIP tests cubic specimens of approximately 1 cm^3, also moulded from intact and compacted (A1, A2, A3, B1, B2 and B3) samples, underwent freezing in liquid nitrogen (-195 °C) and drying in a vacuum oven. MIP tests were performed using the AutoPore IV 9500 equipment from Micromeritics Instrument Corporation.

3. Mineralogical investigation

The morphology and texture of the halloysite mineral vary according to the intensity of the decomposition process and the effects of transport (Heiken and Wohletz, 1992), with the shape of tubes being its predominant morphology (Senoussi et al., 2016). Allophanes, on the other hand, are characterised by small hollow spheres of around 5 nm in diameter, 3.8 nm in internal diameter and holes of around 0.3 nm (Iyoda et al., 2012).

SEM images of intact, A1 and B3 specimens are shown in **Fig. 3**. All three SEM images clearly indicate the existence of tubular structures that are characteristics of the halloysite mineral, while hollow sphere structures, characteristic of allophanes, could not be observed. In all three images, the diameter of the observed halloysite tubes range between 0.1 and 0.3 μm. A structural disorder and clay aggregations can also be observed in the three images.

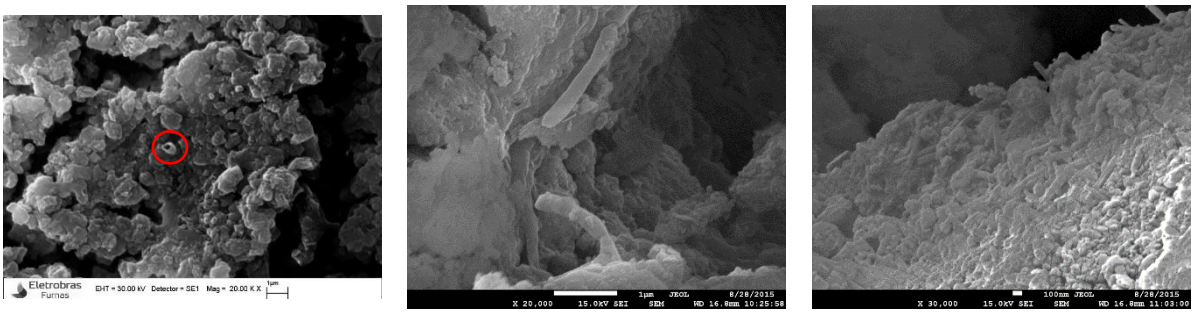

(a) (b) (c)

Fig. 3. *SEM images of (a) Intact sample 20,000× magnification, where circle indicates a tubular structure, (b) A1, 20,000× magnification, and (c) B3, 30,000× magnification.*

Failure to observe allophane in SEM images does not necessarily indicate that allophanes are not present in this material. Further tests need to be carried out to establish the presence or inexistence of allophane. Thus, **Fig. 4** shows the X-Ray Diffraction results of three specimens: oven dried at 105 °C, air dried to the hygroscopic water content and at the natural water content of 78% without drying. The peaks identified in all three samples correspond to: gibbsite (d = 4.84 Å, $CaSO_4.2H_2O$), halloysite (d = 4.36 Å, $Al_2Si_2O_5(OH)_4$), cristobalite (d = 4 Å, SiO_2), quartz (d = 3.34 Å, SiO_2), and kaolinite (d = 2.4 Å, $Al_2Si_2O_5(OH)_4$) (Bordeepong et al., 2011; Deng et al., 2017; Falcón et al., 2015; Joussein et al., 2006; Lizcano et al., 2006; Tchakouté et al., 2020; Wesley, 1973). The main kaolinite peak (d = 7.2 Å) does not appear in any of the results, which indicates that kaolinite is poorly crystallized with disorder on the b axis (Hildebrando et al., 2009).

Halloysite is a hydrated polymorph of kaolinite (Emmanuel et al., 2019; Joussein et al., 2006). Based on its hydration state, halloysite is classified into two groups: the hydrated form (10 Å), and the dehydrated form (7 Å). The peak that characterises hydrated halloysite (d = 10 Å) (Cravero et al., 2016; Deng et al., 2017; Emmanuel et al., 2019; Wesley, 1973) can only be detected in the moist specimen. This finding is not surprising, since halloysite can dehydrate irreversibly at relative low temperatures (Bordeepong et al., 2011). However, it is widely reported in the literature (Bordeepong et al., 2011; Joussein et al., 2005) that this 10 Å halloysite (hydrated) is likely to convert irreversibly into its 7 Å (dehydrated) form. Nevertheless, the peak that characterises dehydrated halloysite (d = 7 Å, $Al_2Si_2O_5(OH)_4$) (Joussein et al., 2005) is absent in all three specimens tested.

Since allophane is characterised by three main peaks at d = 3.3 Å, 2.25 Å and 1.4 Å, that cannot be observed in neither specimen, **Fig. 4** further confirms that allophane is not present in the material tested.

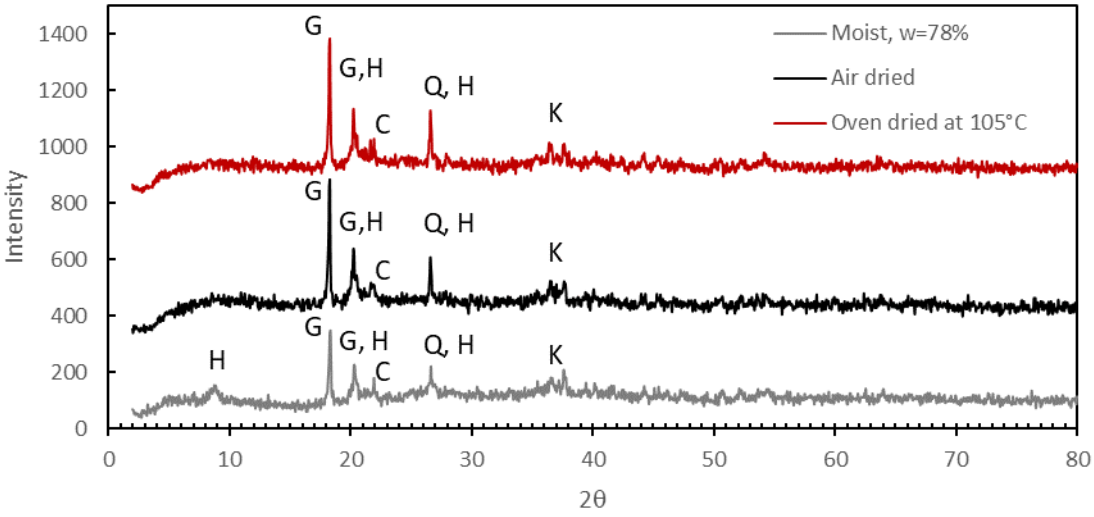

***Fig. 4**. XRD of oven dried; air dried to hydroscopic water content and moist specimens, where H: halloysite, K: kaolinite, G: gibbsite, Q: quartz e C: cristobalite*

To substantiate the XRD analyses, the weight-loss curve (TG) and its differential (DTA) for an intact specimen can be inspected in **Fig. 5**. The DTA of the specimen is characterised by four main thermal events: (1) an endothermic peak at around 50 °C, corresponding to the loss of adsorbed water (surface and interlayer) (Iyoda et al., 2012; Singer et al., 2004) which characterises the dehydration of the halloysite according to Falcón et al. (2015); (2) a second endothermic peak at around 250°C, which corresponds to the dehydration and decomposition of the gibbsite (Falcón et al., 2015); (3) an exothermic peak at 300 °C caused by the detachment of the organic matter (Falcón et al., 2015); (4) and another exothermic peak at 470 °C which is the result of the dehydration of kaolinite (Falcón et al., 2015). From the DTA curve in **Fig. 5**, it can be observed that not much energy is required to remove the water from the halloysite, that is, it can occur at low temperatures.

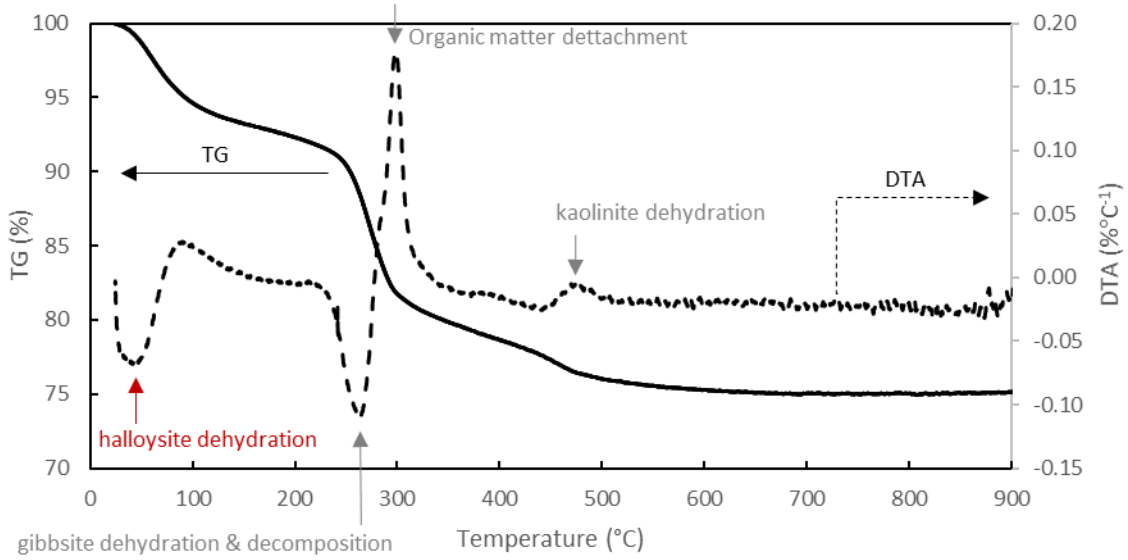

Fig. 5. *Thermal analyses curves (TG/DTA).*

Complementarily to the XRD and TG/DTA analyses, FTIR test was performed on a specimen B (dried to the hydroscopic water content - **Fig. 6**). The absorption bands at 3633, 1047, 948 cm^{-1} correspond to halloysite (Espinoza and Meléndez, 2012; Singer et al., 2004); absorption bands at 3481, 3540 cm^{-1} correspond to gibbsite; strong OH stretching band of adsorbed water between approximately 3450–3550 cm^{-1} (Lun et al., 2014); absorption band at 1640 cm^{-1} relates to the hydroxyl group of water molecules present in the clay (H-O-H bending vibrations) (Polanský et al., 2017) specifically to the deformation of Si-OH bonds, which would be related to the presence of kaolinite (Espinoza and Meléndez, 2012).

The FTIR result confirms the presence of gibbsite, kaolinite and halloysite minerals identified in the XRD and thermal analyses. The wide spectrum of absorption bands of the gibbsite shows that the weathering process allowed the crystallization of this mineral (Espinoza and Meléndez, 2012).

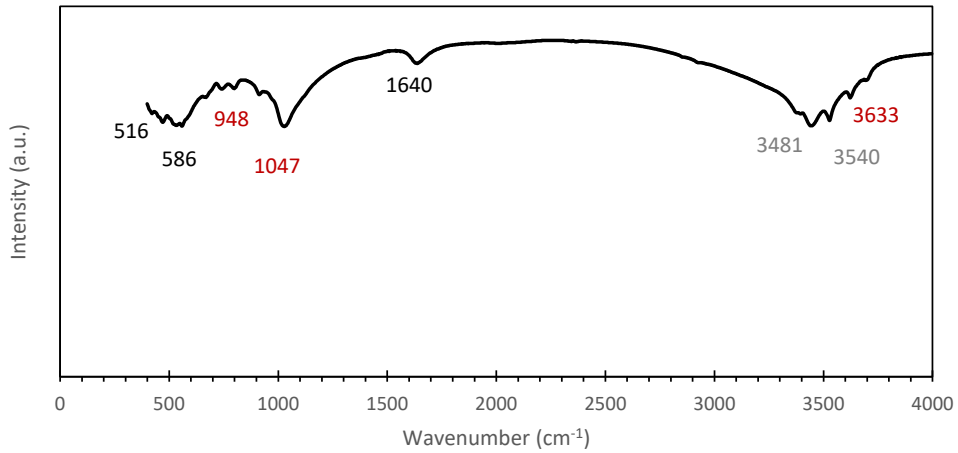

Fig. 6. *FTIR Spectra.*

4. Geotechnical investigation

Fig. 7 shows the particle size distribution of intact specimens and specimens prepared according to procedure B (air-dried to hygroscopic water content) with and without dispersant. The process of air drying to the hygroscopic water content forms aggregations of the finer particles (clay-sized) increasing the amount of sand-sized particles, a result similar to that obtained by Wesley (1973). When comparing the effect of dispersant on specimens prepared under the same conditions, it is observed that the dispersant separates particles, which generates an increase in the amount of silt- and clay-sized particles. However, the use of dispersant does not appear to be enough to erase the aggregation caused by the drying procedure.

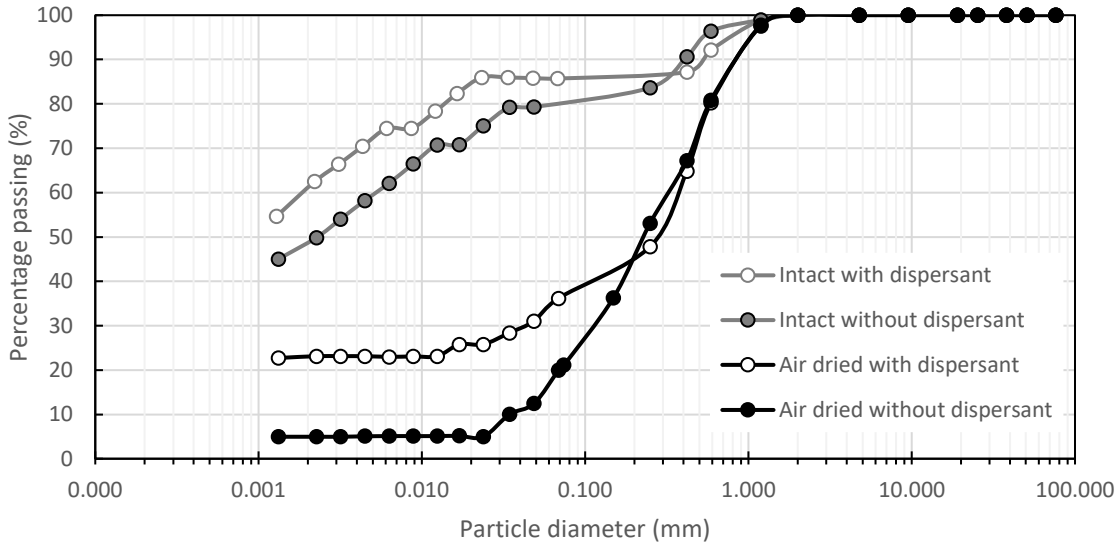

Fig. 7. *Particle size distribution of intact and air-dried samples with and without dispersant.*

The plasticity of the material is influenced by the drying process, as demonstrated in the plasticity chart of **Fig. 8**. Specimens prepared according to the drying procedure B are non-plastic, while intact and specimens prepared according to drying procedure A are plastic. Although specimens A and intact are in the same region of the plasticity chart, there is a slight variation in the liquid limit and plasticity index obtained for these two types of specimens, with the intact specimen exhibiting higher liquid limit and plasticity index.

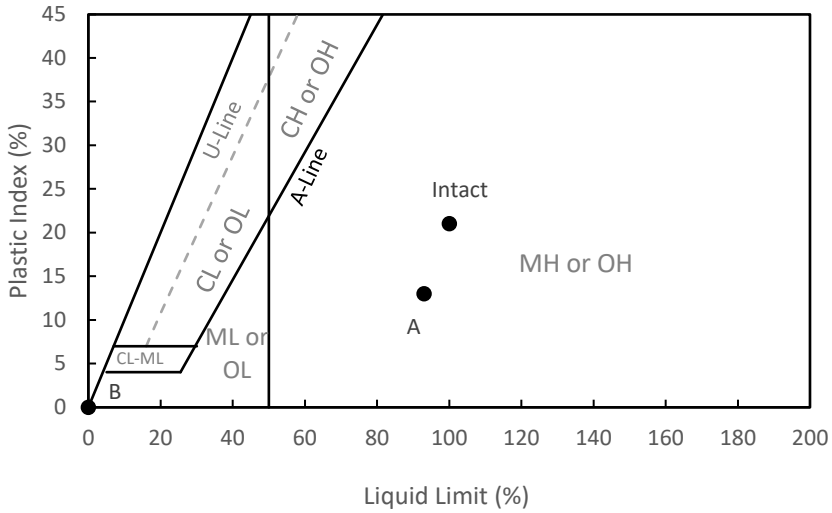

Fig. 8*. Plasticity index chart*

From the results of the particle size distribution and Atterberg limits, according to the Unified Soil Classification System (USCS), the material in an intact state and when it undergoes procedure A of drying can be classified as silt of high plasticity (MH-OH) and when it undergoes procedure B of drying, it is classified as silty sand (SM).

Thus, it is clear that the drying procedures influence the structural arrangement and consequently the classification according to particle size and the Atterberg limits. Similar results were obtained by Ferrari et al. (2013); Herrera (2005); Wesley (2009).

5. Hydromechanical investigation

5.1 Soil Water Retention Curve

Fig. **9** shows the results of the SWRC obtained from the drying and wetting paths on intact and compacted specimens. The drying preparation process has evident effects on three characteristics of the SWRC drying paths, that are: i) shape of the curves; ii) change in the air entry value; and iii) amount of water stored. While specimens prepared under drying procedure A, air-dried to the target water contents before compaction (A1, A2 and A3), show water content values for saturated condition above 65%, specimens prepared under drying procedure B, air-dried to hygroscopic water content before wetting and compaction (B1, B2 and B3), present values close to 50%. In addition, for specimens prepared under drying procedure A, the variation in compaction water content seems to have greater influence than in specimens that have undergone drying procedure B, where no difference is observed between the three samples.

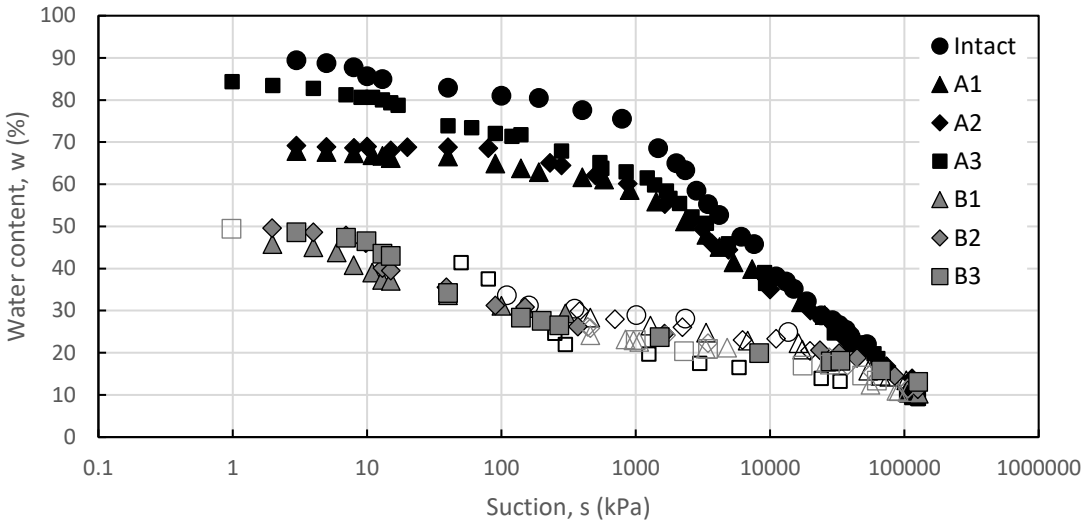

Fig. 9. *Soil Water Retention Curves, where closed symbols indicate drying paths and open symbols indicate wetting paths.*

It is important to note that all A specimens (A1, A2 and A3) absorbed water after saturation (Fig. 9 starting point of drying paths). However, specimen A3 absorbed considerably more water than the other two samples. This behaviour seems to contradict the literature on compacted soils, in the sense that soils compacted on the dry of optimum tend to expand more than soils compacted on the wet of optimum. This apparent contradiction may be a consequence of the fact that the three A specimens are already very close to saturation after compaction and probably have air bubbles occluded; these air bubbles are then more difficult to remove in specimens A1 and A2 than in specimen A3."

Another interesting point highlighted by the SWRC is that specimens A present high hysteresis, while specimens B do not present any hysteresis between the drying and wetting paths. In the drying-wetting cycle, specimens A show that the drying process produces a change in how the water is stored. Additionally, it can be observed that the wetting curves of specimens A, B and intact are almost coincident.

When specimens reach suctions greater than 10 and 20 MPa, at water content close to 40% and 20% for the drying and wetting paths respectively, they begin to converge, which may imply that the air entry value of the mesopores (pores between 0.002 and 0.05µm in diameter, according to IUPAC (1997) is the same regardless of the sample preparation process. Furthermore, despite having silt-sized particles the air entry values of intact and A specimens are high on the drying path.

346 *5.2. Consolidation test*

347 *The saturated compressibility curves are presented in*

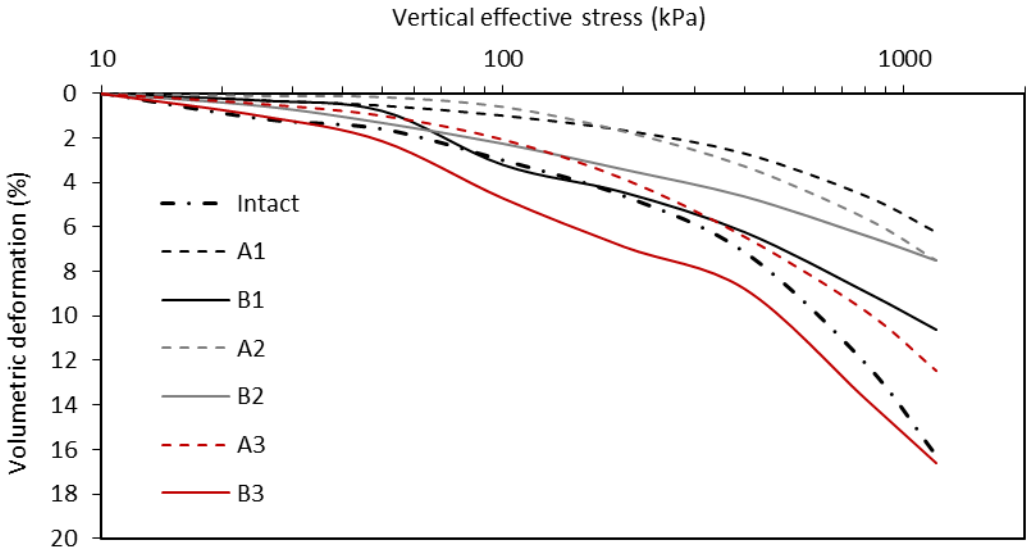

348

349 **Fig. 10** in terms of volumetric deformation to remove the effect of the initial void ratio. Specimen B2
350 (air dried to the hygroscopic water content) at optimum, is the least compressible specimen, while the
351 intact specimen is the most compressible specimen (**Table 2**).

352 *Results presented in*

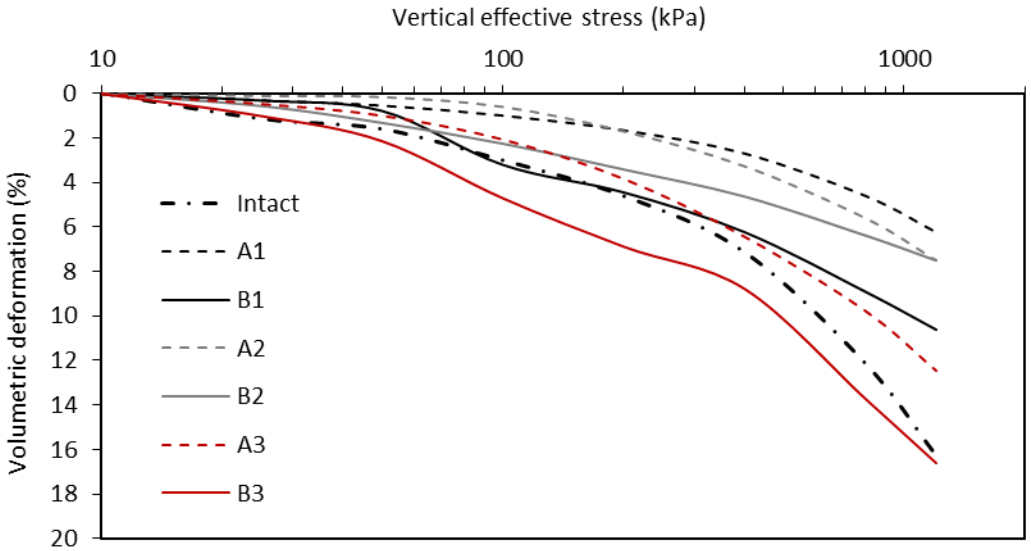

353

354 **Fig. 10** do not provide conclusive evidence about the effects the drying procedures have on the
355 compressibility of the material. However, compressibility tests indicate that compressibility increases
356 in the following way: B2 < A1 < B1 < A2 < A3 < B3 < Intact (**Table 2**).

357

358

359

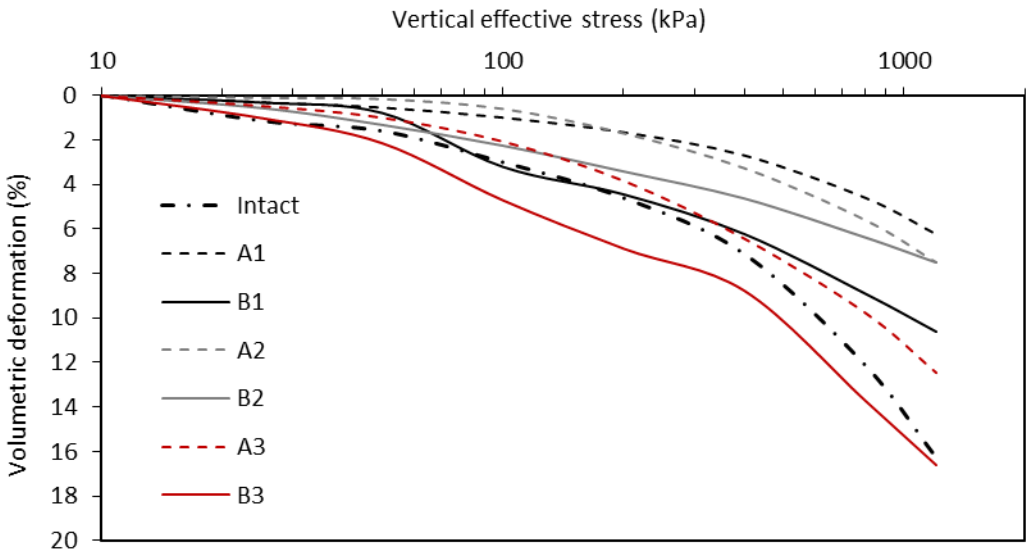

Fig. 10. *Volumetric Deformation.*

Table 2 Compressibility parameters.

Sample	Water content, w (%)	Initial void ratio, e_i	Final void ratio, e_f	Compression index, Cc	Pre-consolidation stress, σ'_p (kPa)
Intact	78.0	2.95	2.43	0.754	250
A1	64.0	1.93	1.82	0.217	240
A2	65.3	1.78	1.64	0.246	190
A3	72.0	1.91	1.57	0.368	180
B1	38.0	1.42	1.24	0.223	92
B2	38.8	1.29	1.14	0.138	130
B3	42.0	1.42	1.03	0.398	180

6. Structural investigation

MIP and Nitrogen absorption tests were carried out in compacted and intact specimens. **Fig. 11** shows the Pore Size Distribution (PSD) curve obtained through the multi-modal fitting, similarly to that proposed by Lopes et al. (2014) of the combined experimental data. A trimodal distribution of pores can be observed in all specimens. According to IUPAC (1997) size classification, two of these peaks are observed in the macropores region, between 1 and 400µm, and between 0.01 and 5µm, and a third peak in the mesopores region, between 0.003 and 0.01µm.

The drying and compaction processes do not seem to have affected the distribution of mesopores; while these processes appear to have played an important role in the distribution of macropores, particularly in the region of the largest pores.

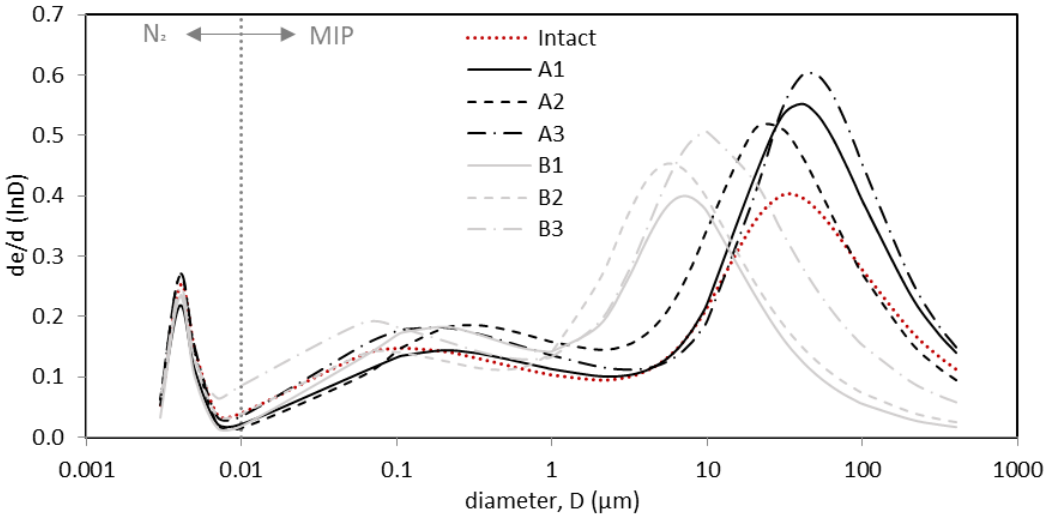

***Fig. 11**. Pore size distribution curves combining MIP and nitrogen adsorption (N_2) techniques.*

In all cases, the void ratios obtained by the combined porosimetry tests were lower than the void ratios of the specimens presented in Table 1. This is a common issue reported by many researchers on porosimetry test carried out in different clayey soil samples (Cordão Neto et al., 2018; Kühn et al., 2021; Lopes, 2016; Pedrotti, 2016; Romero and Simms, 2008) and it could be mainly associated with (i) isolated pores surrounded by solids which are not intruded; (ii) some pores which are accessible only through smaller pores, i.e., they are not detected until smaller pores are penetrated, restricted porosity.

Isotherms were also obtained from Nitrogen adsorption and desorption tests. All isotherms belong to type IV with H3 hysteresis (**Fig. 12**) loops between adsorption and desorption curves (Gregg and Sing, 1982; Sing and Williams, 2004; Yuan et al., 2012). According to Teixeira et al. (2001) when condensation occurs inside the pores, where the forces of attraction are greater due to the proximity between the molecules, it can occur at lower pressures than in non-porous solids. Evaporation, however, is hampered by the shape of the pore. Thus, the different paths characterise a hysteresis between the adsorption and desorption processes.

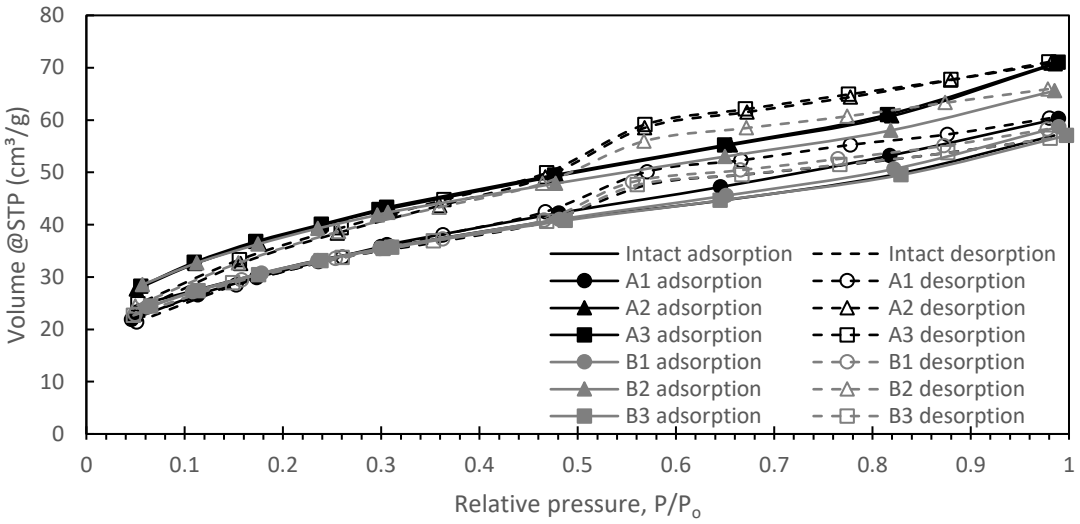

***Fig. 12**. Isotherms of adsorption and desorption of nitrogen.*

Also from the Nitrogen adsorption test, the specific surface of the specimens could be calculated by the BET method (**Table 3**). The compacted specimens at optimum water content and the intact specimen exhibit the highest specific surface values.

***Table 3** Specific surface of samples.*

Sample	Specific surface (m²/g)
Intact	126.04
A1	109.07
A2	130.22
A3	119.14
B1	108.06
B2	128.24
B3	107.58

7. Discussions

SEM images together mineralogical analyses of the volcanic ash under investigation did not reveal evidence that suggest allophane is present in the soil. However, these tests did indicate that halloysite is present in the soil composition. Halloysite tubes could be observed in SEM images of intact samples as well as samples subjected to drying procedure A, which involves air drying the disturbed soil up to the target water content required, and procedure B, which involves air drying the disturbed soil to the hygroscopic water content.

Based on its hydration state, halloysite is classified into two groups: the hydrated form (d = 10 Å), and the dehydrated form (d = 7 Å). Halloysite-(10 Å) can easily and irreversibly dehydrate giving rise to halloysite-(7 Å), because the interlayer water is weakly held. XRD test on moist samples (**Fig. 4**) shows

a peak at 10 Å and no peak at 7 Å, thus indicating the presence of hydrated halloysite. However, XRD tests on air dried and oven dried (at 105 °C) samples did not reveal peaks at 10 Å or 7 Å. Nevertheless, XRD test on all these three samples indicated other characteristic halloysite peaks (d = 4.36 Å and 3.35 Å). Furthermore, mineralogical tests also indicated the presence of halloysite in this soil.

The compaction behaviour changes completely depending on the drying procedure adopted (**Fig. 2**). For performing standard compaction tests in the laboratory, samples collected are first subject to air drying to the hygroscopic water content, and then the optimum water content and maximum dry unit weight are determined. In contrast, when this material is compacted in the field, it is not first subjected to drying to the hygroscopic water content. Instead, the natural water content is accessed and then water is either added to the material, if this natural water content is lower than the optimum determined in the lab, or the material is dried by revolving the soil, if the natural water content is higher than the optimum. Popayán volcanic ash when compacted in laboratory following standard drying to the hygroscopic water content presented the optimum water content and dry unit weight of 38.8% and 11.31kN/m^3, respectively, while when this material was compacted in the lab and dried only to the target water content the optimum water content and dry unit weight obtained were 65.3% and 9.32kN/m^3, respectively. This demonstrates that compaction specifications determined in the lab following standard procedures drive compaction conditions in the field excessively on the dry of optimum. This in turn could inadvertently lead to undesired engineering properties.

This remarkable contrast in compaction behaviour has already been brought to light by previous studies on volcanic soils (Hernandez et al., 2018; Wesley, 2009). These studies attributed the difference in behaviour to the existence of either allophane and/or halloysite. According to the authors the drying process irreversibly removes water at mineral scale, which then leads to a different structure able to sustain less water.

Additionally, the loss of water at mineral level appears to have other consequences. The process of air drying to the hygroscopic water content forms strongly held aggregations (D50 = 0.002mm and 0.25mm for natural water content and air dried to hygroscopic water content respectively) that are only marginally broken when dispersants are used (**Fig. 7**), while also changing the plasticity from plastic (dried to target water contents) to non-plastic (dried to hygroscopic water content first) (**Fig. 8**).

Another interesting point highlighted by the SWRC (**Fig. 9**) is that intact and A (dried to target water contents) specimens present high hysteresis, while B specimens (dried to hygroscopic water content) do not present any hysteresis between the drying and wetting paths. This suggests that when water leaves the mineral structure, it cannot be reincorporated in a wetting process. Specimens B, on the

other hand, had this loss of interlayer water anticipated during the sample preparation process. Additionally, the fact that the wetting curves of specimens A, B and intact are almost coincident reinforces the idea that the difference between the wetting and drying paths is mainly due to the water leaving the mineral structure and not only the water leaving the pores (Inoue et al., 2012). Therefore, it is reasonable to assume that the effect of the observed hysteresis is related to the loss of the interlayer water (Kamble et al., 2012). This is another evidence, along with the change in Atterberg Limits, which demonstrate the influence of interlayer water on soil behaviour.

Furthermore, despite having silt-sized particles the air entry values of intact and A specimens are high on the drying path (Fig. **9**). This behaviour is the opposite of what is expected, since intact and A specimens have macropore diameters larger than specimens B (Fig. **11**). Nevertheless, water remains stored in intact and A specimen's pores for higher suction values than in B specimens. The presence of hydrated halloysite may explain the great difference in the hydraulic properties of the soil, influencing the water retention capacity (the water leaving the inside of the tubular structure of the halloysite structure is an irreversible process) and affecting the strong connections between particles (Nanzyo et al., 1989; Tadashi and SHoji, 2002; Wesley, 2009, 1973, 2014). Understanding whether this difference relates to the water stored in pores or to the water stored inside the mineral is fundamental to understand the hydromechanical behaviour of this material.

At first sight, results of the distribution of pores presented in **Fig. 11** disagree with the particle size distribution and SWRC (drying paths) results. **Fig. 11** indicated that the drying procedure B, to the hygroscopic water content, reduces the largest dominant pore size of the macropores (from 25 µm to 5 µm, average dominant macro pore size of group A and B respectively). Despite that, particle size distribution results indicated that particles of samples that followed drying procedure B are larger in diameter than the intact samples' particles, hence it can be automatically assumed that the pores of B samples are larger than intact samples. Similarly, the suction at air entry values of B samples is smaller than intact and A samples, which suggests once more that B samples have larger pores.

A more in-depth examination might help reconcile these results. It has been already stablished that when halloysite is in its hydrated form it stores water in its interlayer. Once water drains out of the interlayer it cannot be restored, hence the observations made via the SWRC, i.e.: (A) the air entry value suction of intact and A samples is greater than in B samples in the drying paths; (B) the hysteresis between the drying and wetting paths of intact and A samples; (C) the lack of hysteresis between the drying and wetting paths of B samples; and (D) the fact that the curves of intact, A and B samples in the wetting paths are almost coincident. A by-product of the water leaving permanently the halloysite layers has been demonstrated by Kohyama et al. (1978). The authors showed evidence that the rolled layers of tubular halloysite, originally tightly connected to each other, became separated as a result of

dehydration. Then, since halloysites (10 Å or 7 Å) are found in the form of aggregates from an early stage in their formation (Jeong, 1998), the aggregates that contain halloysite particles increase in size, hence the largest particle size of B samples observed in the particle size distribution. Following this increase in aggregates size comes a reduction in the size of macropores, as observed in **Fig. 11**.

The drying procedures appear to have affected less the compressibility of the samples. The differences observed are inconclusive. However, the high compressibility of the intact sample may be explained by the loss of the original cemented structure. According to Lizcano et al. (2006) cementation of volcanic soils is mainly given by the presence of minerals from the clay fraction, such as halloysite or allophane. Wesley (2003) suggested that when these soils dry, the cemented structure deteriorates.

Similarly, the isolated analysis of the specific surface data presented in **Table 3** does not indicate any special behaviour, since the range of variation could be considered a dispersion around the mean (mean = 118.34m²/g and standard deviation = 10.05 m²/g). However, liquid limit and plasticity index results (**Fig. 8**) demonstrate a wide variation in the way the particles interact with water, and this behaviour is strongly influenced by the specific surface. This behaviour could be associated with the loss of water (irreversible process) at mineral level.

8. Conclusions

Results of an experimental investigation carried out on a volcanic soil from Popayan, Colombia, were presented here to investigate the extent to which changes in drying affect the engineering behaviour of the soil. Mineralogical, geotechnical, hydromechanical, and structural tests were performed.

Mineralogical tests indicated the presence of halloysite, gibbsite, kaolinite, quartz and cristobalite in the soil. From the geotechnical, hydromechanical and structural tests it was possible to recognise that the drying procedure influenced: compaction behaviour; consistency limits; particle size distribution; retention behaviour; compressibility and pore size distribution (> 1 μm), while not having great effect on: specific surface; pore size distribution (< 1 μm).

Combined analyses of the laboratory tests performed suggested that the dehydration of halloysite at mineral scale could then explain the distinct change in engineering behaviour observed when this soil is subjected to drying.

Acknowledgments

The authors would like to thank Eletrobrás Furnas for the support provided to carry out this research.

References

Almazán, D., 2013. Experiencia en el empleo de cenizas para la construcción de terraplenes y explanadas en el enlace de acceso al Hospital Universitario de Asturias. Carreteras 187, 95–104.

American Society for Testing and Materials. ASTM D2435/D2435M, 2020. Standard Test Methods for One-Dimensional Consolidation Properties of Soils Using Incremental Loading.

American Society for Testing and Materials. ASTM D4318-17, 2017. Standard Test Methods for Liquid Limit, Plastic Limit, and Plasticity Index of Soils. West Conshohocken, PA.

American Society for Testing and Materials. ASTM D6913 / D6913M-17, 2017. Standard Test Methods for Particle-Size Distribution (Gradation) of Soils Using Sieve Analysis. West Conshohocken, PA.

American Society for Testing and Materials. ASTM D7928, 2017. ASTM D7928-17 Standard Test Method for Particle-Size Distribution (Gradation) of Fine-Grained Soils Using the Sedimentation (Hydrometer) Analysis, Annual book of ASTM standards 2017. https://doi.org/10.1520/D7928-17

American Society for Testing and Materials. ASTM D854-14, 2014. Standard Test Methods for Specific Gravity of Soil Solids by Water Pycnometer. West Conshohocken, PA.

Associação Brasileira de Normas Ténica. NBR 7182, 2016. Ensaio de compactaçao. Rio de Janeiro.

ASTM D698, 2012. Standard Test Methods fLaboratory Compaction Characteristics of Soil Using Standard Effort (12 400 ft-lbf / ft 3 (600 kN-m / m 3)) 1. https://doi.org/10.1520/D0698-12.1.4

Bartoli, F., Begin, J.., Burtin, G., Schouller, E., 2007. Shrinkage of initially very wet soil blocks , cores and clods from a range of European Andosol horizons. Eur. J. Soil Sci. 58, 378–392. https://doi.org/10.1111/j.1365-2389.2006.00889.x

Betancur, Y., Builes, M., Millán, A., 2013. Variación de las propiedades mecánicas de arcillas alófanas en colombia al variar el grado de saturación. Rev. EIA 10, 173–181.

Bommer, J.J., Rolo, R., Mitroulia, A., Berdousis, P., 2002. Geotechnical Properties and Seismic Slope Stability of Volcanic Soils, in: 12th European Conference on Earthquake Engineering.

Bordeepong, S., Bhongsuwan, D., Pungrassami, T., Bhongsuwan, T., 2011. Characterization of halloysite from thung yai district, Nakhon Si Thammarat Province, in Southern Thailand. Songklanakarin J. Sci. Technol. 33, 599–607.

Colombo, C., Sellitto, V.M., Palumbo, G., Di Iorio, E., Terribile, F., Schulze, D.G., 2014. Clay formation and pedogenetic processes in tephra-derived soils and buried soils from Central-Southern

533 Apennines (Italy). Geoderma 213, 346–356. https://doi.org/10.1016/j.geoderma.2013.08.005

534 Cordão Neto, M.P., Hernández, O., Lorenzo Reinaldo, R., Borges, C., Caicedo, B., 2018. Study of the
535 relationship between the hydromechanical soil behavior and microstructure of a structured soil.
536 Earth Sci. Res. J. 22, 91–101. https://doi.org/10.15446/esrj.v22n2.65640

537 Cravero, F., Fernández, L., Marfil, S., Sánchez, M., Maiza, P., Martínez, A., 2016. Spheroidal halloysites
538 from Patagonia, Argentina: Some aspects of their formation and applications. Appl. Clay Sci. 131,
539 48–58. https://doi.org/10.1016/j.clay.2016.01.011

540 De Vita, P., Di Maio, R., Piegari, E., 2012. A study of the correlation between electrical resistivity and
541 matric suction for unsaturated ash-fall pyroclastic soils in the Campania region (southern Italy).
542 Environ. Earth Sci. 67, 787–798. https://doi.org/10.1007/s12665-012-1531-4

543 Deng, L., Yuan, P., Liu, D., Annabi-bergaya, F., Zhou, J., 2017. Effects of microstructure of clay minerals,
544 montmorillonite, kaolinite and halloysite, on their benzene adsorption behaviors. Appl. Clay Sci.
545 143, 184–191. https://doi.org/10.1016/j.clay.2017.03.035

546 Dorel, M., Roger-Estrade, J., Manichon, H., Delvaux, B., 2000. Porosity and soil water properties of
547 Caribbean volcanic ash soils. Soil Use Manag. 16, 133–140.

548 Dörner, J., Dec, D., Peng, X., Horn, R., 2009. Change of shrinkage behavior of an Andisol in southern
549 Chile: Effects of land use and wetting/drying cycles. Soil Tillage Res. 106, 45–53.
550 https://doi.org/10.1016/j.still.2009.09.013

551 Emmanuel, E., Lau, C.C., Anggraini, V., Pasbakhsh, P., 2019. Stabilization of a soft marine clay using
552 halloysite nanotubes: A multi-scale approach. Appl. Clay Sci. 173, 65–78.
553 https://doi.org/10.1016/j.clay.2019.03.014

554 Espinoza, D., Meléndez, W., 2012. Geochemical Study of Neoformed Minerals Present in the Bauxite
555 of Los Pijiguaos , Venezuela. Rev. la Fac. Ing. U.C.V 27, 39–52.

556 Falcón, J.M., Sawczen, T., Aoki, I.V., 2015. Dodecylamine-Loaded Halloysite Nanocontainers for Active
557 Anticorrosion Coatings. Front. Mater. 2, 1–13. https://doi.org/10.3389/fmats.2015.00069

558 Ferrari, A., Eichenberger, J., Laloui, L., 2013. Hydromechanical behaviour of a volcanic ash.
559 Géotechnique 63, 1433–1446. https://doi.org/10.1680/geot.13.P.041

560 Gregg, S.., Sing, K.S.., 1982. Adsorption, Surface Area and Porosity, 2nd Editio. ed. Academic Press,
561 London.

562 Heiken, G., Wohletz, K.H., 1992. Volcanic Ash, second ed. ed. University of California Press, Berkeley,
563 California.

564 Hernandez, O., Neto, M.P.C., Caicedo, B., 2018. Structural features and hydro-mechanical behaviour
565 of a compacted andesitic volcanic soil. Géotechnique Lett. 8, 1–6.
566 https://doi.org/https://doi.org/10.1680/jgele.18.00056

567 Herrera, M.C., 2005. Suelos derivados de cenizas volcánicas en Colombia: Estudio fundamental e
568 implicaciones en ingeniería. Tesis de doctorado, Departamento de Ingeniería Civil y Ambiental,
569 Universidad de Los Andes, 265 p.

570 Hildebrando, E.A., Sheller, T., Ang, R.S., Neves, R.F., 2009. Caracterização mineralógica de material
571 argiloso proveniente do município de santa bárbara – PA, in: Congresso Brasileiro de Cerâmica.
572 pp. 1–8.

573 Hurtado, G., 2014. Análisis del comportamiento promedio y tendencias de largo plazo de la
574 temperatura máxima media para las regiones hidroclimáticas de Colombia. Colombia.

575 Inoue, A., Utada, M., Hatta, T., 2012. Halloysite-to-kaolinite transformation by dissolution and
576 recrystallization during weathering of crystalline rocks. Clay Miner. 47, 373–390.
577 https://doi.org/10.1180/claymin.2012.047.3.08

578 IUPAC, 1997. '"IUPAC Compendium of Chemical Terminology"' (Gold Book), Blackwell. ed.

579 Iyoda, F., Hayashi, S., Arakawa, S., Okamoto, M., Hayashi, H., Yuam, G., 2012. Synthesis and adsorption
580 characteristics of hollow spherical allophane nano-particles. Appl. Clay Sci. 56, 77–83.
581 https://doi.org/10.1063/1.4873773

582 Jeong, G., 1998. Formation of vermicular kaolinite from halloysite aggregates in the weathering of
583 plagioclase. Clays Clay Miner. 46, 270–279. https://doi.org/10.1346/ccmn.1998.0460306

584 Joussein, E., Petit, S., Churchman, J., Theng, B., Righi, D., Delvaux, B., 2005. Halloysite clay minerals –
585 a review. Clay Miner. 40, 383–426. https://doi.org/10.1180/0009855054040180

586 Joussein, E., Petit, S., Fialips, C.I., Vieillard, P., Righi, D., 2006. Differences in the dehydration-
587 rehydration behavior of halloysites: New evidence and interpretations. Clays Clay Miner. 54,
588 473–484. https://doi.org/10.1346/CCMN.2006.0540408

589 Kamble, R., Ghag, M., Gaikawad, S., Panda, B.B.K., 2012. Halloysite nanotubes and ap- plications: a
590 review. Adv. Sci. Res. 3, 25–29.

591 Kitagawa, Y., 1971. The "unit particle" of allophane. Am. Miner. 56, 465–475.

592 Kohyama, N., Fukushima, K., Fukami, A., 1978. Observation of the hydrated form of tubular halloysite
593 by an electron microscope equipped with an environmental cell. Clays Clay Miner. 26, 25–40.

594 Kühn, V. de O., Lopes, B. de C.F.L., Caicedo, B., Cordão-Neto, M.P., 2021. Micro-structural and

595 volumetric behaviour of bimodal artificial soils with aggregates. Eng. Geol. 288, 106139.
596 https://doi.org/https://doi.org/10.1016/j.enggeo.2021.106139

597 Lizcano, A., Herrera, M.C., Santamarina, J.., 2006. Suelos derivados de cenizas volcánicas en colombia.
598 Rev. Int. Desastr. Nat. Accid. e Infraestruct. Civ. 6, 167–198.

599 Lopes, B., 2016. Microstructural based approach to the modelling of clays and transitional soils
600 behaviour. Tese de doutorado, Departamento de Engenharia Civil e Ambiental,Universidade de
601 Brasília, Brasília, 133p.

602 Lopes, B., Neto, M., Tarantino, A., 2014. An approach to detect microand macro-porosity from MIP
603 data. Unsaturated Soils Res. Appl. 685–689. https://doi.org/10.1201/b17034-96

604 Lun, H., Ouyang, J., Yang, H., 2014. Enhancing dispersion of halloysite nanotubes via chemical
605 modification. Phys. Chem. Miner. 41, 281–288. https://doi.org/10.1007/s00269-013-0646-9

606 Matsumura, S., Miura, S., Yokohama, S., Kawamura, S., 2015. Cyclic deformation-strength evaluation
607 of compacted volcanic soil subjected to freeze-thaw sequence. Soils Found. 55, 86–98.
608 https://doi.org/10.1016/j.sandf.2014.12.007

609 Nanzyo, M., Shoji, S., Dahlgren, R., 1989. Physical characteristics of volcanic ash soils, in: Physical
610 Characteristics of Volcanic Ash Soils. pp. 189–207.

611 Neall, V.E., 2009. Land use and land cover and soil sciences, in: Volcanic Soils. pp. 23–45.

612 Pedrotti, M., 2016. An experimental investigation on the micromechanisms of non-active clays in
613 saturated and partially saturated states. PhD. Thesis, University of Strathclyde.

614 Polanský, R., Kadlec, P., Kolská, Z., Š, V., 2017. Influence of dehydration on the dielectric and structural
615 properties of organically modified montmorillonite and halloysite nanotubes. Appl. Clay Sci. 147,
616 19–27. https://doi.org/10.1016/j.clay.2017.07.027

617 Poulenard, J., Podwojewski, P., Herbillon, A.J., 2003. Characteristics of non-allophanic Andisols with
618 hydric properties from the Ecuadorian páramos. Geoderma 117, 267–281.
619 https://doi.org/10.1016/S0016-7061(03)00128-9

620 Romero, E., Simms, P.H., 2008. Microstructure investigation in unsaturated soils: A review with special
621 attention to contribution of mercury intrusion porosimetry and environmental scanning electron
622 microscopy. Geotech. Geol. Eng. https://doi.org/10.1007/s10706-008-9204-5

623 Senoussi, H., Osmani, H., Courtois, C., Bourahli, M.E.H., 2016. Mineralogical and chemical
624 characterization of DD3 kaolin from the east of Algeria. Bol. la Soc. Esp. Ceram. y Vidr. 55, 121–
625 126. https://doi.org/10.1016/j.bsecv.2015.12.001

626 Shah, P., Singh, D., 2005. Methodology for determination of hygroscopic moisture content of soils. J.
627 ASTM Int. 3, 1–14. https://doi.org/10.1520/jai13376

628 Shoji, S., Nanzyo, M., Dahlgren, R.A., 1993. Volcanic Ash Soils: genesis, properties and utilization.

629 Sing, K.S.W., Williams, R.T., 2004. The use of molecular probes for the characterization of nanoporous
630 adsorbents. Part. Part. Syst. Charact. 21, 71–79. https://doi.org/10.1002/ppsc.200400923

631 Singer, A., Zarei, M., Lange, F.M., Stahr, K., 2004. Halloysite characteristics and formation in the
632 northern Golan Heights. Geoderma 123, 279–295.
633 https://doi.org/10.1016/j.geoderma.2004.02.012

634 Soil Survey Staff, 1998. Keys to Soil Taxonomy, 8th edition. USDA-NRCS, Soil Survey Sta.

635 Tadashi, A., SHoji, S., 2002. Distribution and Classification of Volcanic Ash Soils. Glob. Environ. Res. Ed.
636 6, 83–97.

637 Tchakouté, H.K., Melele, S.J.K., Djamen, A.T., Kaze, C.R., Kamseu, E., Nanseu, C.N.P., Leonelli, C.,
638 Rüscher, C.H., 2020. Microstructural and mechanical properties of poly(sialate-siloxo) networks
639 obtained using metakaolins from kaolin and halloysite as aluminosilicate sources: A comparative
640 study. Appl. Clay Sci. 186, 105448. https://doi.org/10.1016/j.clay.2020.105448

641 Teixeira, V.G., Coutinho, F.M.B., Gomes, A.S., 2001. Principais Métodos de Caracterização da
642 Porosidade de Resinas à Base de Divinilbenzeno. Quim. Nova 24, 808–818.

643 Terlien, M.T.J., 1997. Hydrological landslide triggering in ash-covered slopes of Manizales (Colombia).
644 Geomorphology 20, 165–175.

645 Wesley, L., 2009. Behaviour and geotechnical properties of residual soils and allophane clays. Obras y
646 Proy. 5–10.

647 Wesley, L., 2003. Geotechnical characterization and behavior of allophone clays. Characterisation and
648 engineering properties of natural soils, Tan et al. ed. Lisse.

649 Wesley, L., 1973. Some basic engineering properties of halloysite allophane clays in Java , Indonesia.
650 Géotechnique 23, 471–494.

651 Wesley, L.D., 2014. Classification and Characterisation of Tropical Residual Soils, in: XIV Congreso
652 Colombiano de Geotecnia. Bogotá, pp. 1–15.

653 Yuan, P., Tan, D., Nnabi-Bergaya, F., Yan, W., Fan, M., Liu, D., He, H., 2012. Changes in structure,
654 morphology, porosity, and surface activity of mesoporous halloysite nanotubes under heating.
655 Clays Clay Miner. 60, 561–573. https://doi.org/10.1346/CCMN.2012.0600602

656